

Turbulent mixing of multiphase flow

By Y.-N. Young
J. Ferziger, F. E. Ham and M. Herrmann

1. Motivation and objectives

Mixing of multi-phase fluids is common in diverse research fields, and understanding of such an important phenomenon is useful to a range of engineering applications such as the polymer blender or control and designs of fluid processing. In this paper we adopt the phase-field modeling approach to investigate capillary induced effects on mixing. Phase-field modeling has been applied to simulation of multi-phase flow (Chella & Vinals 1996; Jasnow & Vinals 1996; Jacqmin 1999) due to its attractive aspect of easy numerical implementation. More recently it has also been applied to simulations of solidification of dendritic alloys (Zhao *et al.* 2003) and polymer blenders (Roths *et al.* 2002).

On macroscopic scales, the interface between two fluids is infinitely sharp. In phase-field modeling, the fluid properties are modeled (assumed) to change smoothly over a small layer across the interface on mesoscopic scales (Chella & Vinals 1996; Jasnow & Vinals 1996). Such a diffuse interface of separation is first considered in a liquid near or at its critical point, where the fluid property within the boundary needs to be modeled and resolved (Siggia 1979). However, phase-field modeling is not restricted to liquids at or near the critical point (Chella & Vinals 1996; Jasnow & Vinals 1996; Jacqmin 1999; Young *et al.* 2003). In fact, one can certainly envision that on the time scale of macroscopic fluid motions, the thermodynamic potential may depend on the gradient of the order parameter, which designates the fluid phase (or density). Accordingly, the macroscopic jump in the normal stress across the interface due to surface tension can be modeled as a mesoscopic continuum body force proportional to gradient of surface potential. On the mesoscopic scales, such a continuum surface tension force varies smoothly in the transition region around the interface. Naturally such a smooth continuum model of fluid interface brings great numerical convenience. Recently, phase-field modeling is made exactly energy-conserving by adding a thermodynamical constraint (Jamet *et al.* 2002). We did not include this constraint in this work as the correction is small for our cases of interest.

An interesting finding in multiphase fluids stirred by chaotic mixing flow is the self-similar drop size distribution (Berthier *et al.* 2001; Muzzio *et al.* 1991*b*). After rescaling the drop size distribution with respect to the characteristic size, all the drop size distributions collapse to a universal functional form for various combinations of parameters, such as viscosity, capillary number, and stirring flow strength. Some explanation to the self-similarity is provided in (Muzzio *et al.* 1991*a,c*), and it is not obvious if similar collapse of size distribution can also be found in a more general turbulent flow, where the distribution of stretching and stretching rate is randomly distributed. In the case of stochastic mixing (Lacasta *et al.* 1995), the existence of a characteristic domain size is an indication that similar collapse of drop size distribution may be found. However, no report on the self-similar drop size distribution is given in Lacasta *et al.* (1995). Thus we conduct numerical simulations of multiphase fluids stirred by two-dimensional turbulence to assess the possibility of self-similar drop size distribution in turbulence. In our

turbulence simulations, we also explore the non-diffusive limit, where molecular mobility for the interface is vanishing. Special care is needed to transport the non-diffusive interface. Numerically, we use the particle level set method to evolve the interface. Instead of using the usual methods to calculate the surface tension force from the level set function, we reconstruct the interface based on phase-field modeling, and calculate the continuum surface tension forcing from the reconstructed interface.

This paper is organized as follows. In §2 we formulate the coupled Navier-Stokes-Cahn-Hilliard system and present results from direct numerical simulations of the coupled system stirred by turbulent flows. In §3.1 we formulate the multiphase fluid problem combining the particle level set method (for interface tracking) with phase-field modeling (for surface tension force). Numerics for the particle level set method are summarized in §3.2, and validation is provided in §3.3. In §3.4 we present results of drop dynamics from direct numerical simulations, and finally we provide some conclusion in §4.

2. Turbulent mixing in the Navier-Stokes-Cahn-Hilliard system

We generalize the system in Berthier *et al.* (2001) to include the effect of surface tension on stirring flows. The phase-field function C denotes the phase of the fluid: $C = \pm 1$ corresponds to fluid phase 1 and 2, respectively. C is described by the Cahn-Hilliard equation, which is coupled to the incompressible, two-dimensional Navier-Stokes equations in our formulation.

$$\frac{\partial C}{\partial t} + \mathbf{u} \cdot \nabla C = \beta \mathcal{M} \nabla^2 \psi, \quad (2.1)$$

$$\frac{\partial \mathbf{u}}{\partial t} + \mathbf{u} \cdot \nabla \mathbf{u} = -\nabla P + \nu \nabla^2 \mathbf{u} - C \nabla \psi + \mathbf{F} + \mathbf{F}_d, \quad (2.2)$$

$$\nabla \cdot \mathbf{u} = 0, \quad (2.3)$$

where

$$\psi(C) \equiv \frac{\delta F(C)}{\delta C} - \frac{\alpha}{\beta} \nabla^2 C, \quad F(C) = \frac{1}{4}(C^2 - 1)^2. \quad (2.4)$$

In equation 2.2, \mathbf{F} is a random forcing at wavenumber k in the range $n_1 \leq k/k_0 \leq n_2$, where $k_0 \equiv 2\pi/l$ and l is the dimension of the computation domain. $\mathbf{F}_d = -\lambda \mathbf{u}$ ($\lambda = 0.1$ in all our simulations) is the drag force dissipating energy at large scales.

The positive, constant coefficient \mathcal{M} is the molecular mobility, ν is the kinematic viscosity, α and β are related to the interfacial properties: The interfacial thickness $\xi \sim \sqrt{\alpha/\beta}$, and the surface tension coefficient $\sigma = \frac{2}{3}\rho_0\sqrt{\alpha\beta} \equiv \sqrt{\alpha\beta}\sigma_0$, where ρ_0 is the uniform fluid density and σ_0 is the surface tension force when $\sqrt{\alpha\beta} = 1$. We can non-dimensionalize the above equations with respect to a characteristic length scale l (of the order of interfacial thickness), a characteristic velocity v_0 , and the corresponding time l/v_0 . The dimensionless equations are

$$\frac{\partial C}{\partial t} + \mathbf{u} \cdot \nabla C = D \nabla^2 [C^3 - C - \nabla^2 C], \quad (2.5)$$

$$\frac{\partial \mathbf{u}}{\partial t} + \mathbf{u} \cdot \nabla \mathbf{u} = -\nabla P + \frac{1}{Re} \nabla^2 \mathbf{u} - \frac{\gamma}{Re} C \nabla [C^3 - C - \nabla^2 C] + \mathbf{F}' + \mathbf{F}'_d, \quad (2.6)$$

$$\nabla \cdot \mathbf{u} = 0. \quad (2.7)$$

The dimensionless coefficient $D \equiv \beta \mathcal{M}/v_0 l$ is the inverse Peclet number, $Re \equiv v_0 l/\nu$ is the Reynolds number, and $\gamma \equiv \sqrt{\alpha\beta}/v_0 \nu$ is the capillary number. If the scaling length

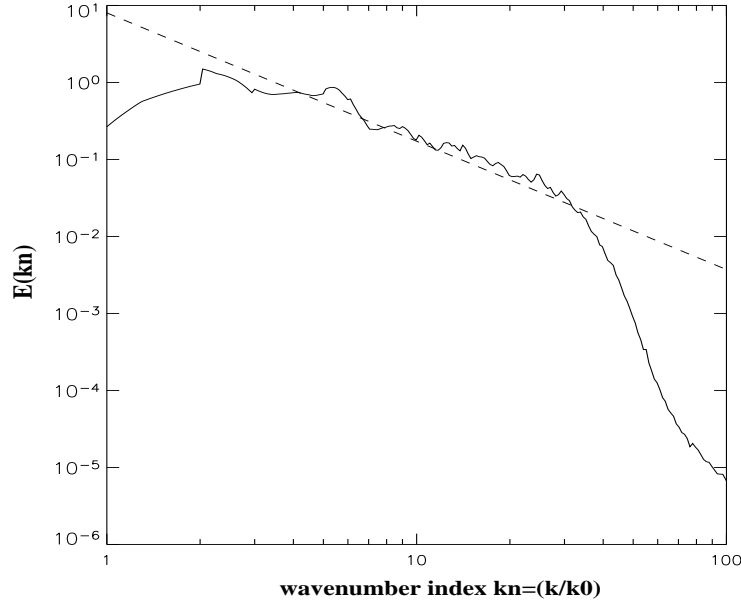


FIGURE 1. Energy spectrum of turbulent velocity (solid line), and the $k^{-5/3}$ inverse cascade scaling is the dashed line. $k_0 = \frac{2\pi}{8\pi} = 1/4$.

scale l is the interfacial thickness ($l \equiv \xi$) and the characteristic velocity is the “diffusion velocity” across the interface ($v_0 \equiv \beta\mathcal{M}/\xi$), then the Reynolds number $Re = \beta\mathcal{M}/\nu$ and the capillary number $\gamma = \alpha/\beta\mathcal{M}\nu$. The time scale for diffusion across the interface is $\tau_C \equiv \xi^2/\beta\mathcal{M}$. The characteristic hydrodynamic time scale is $\tau_S \equiv 1/|\mathbf{S}|$, where $|\mathbf{S}|$ is the velocity strain rate. It is convenient to control the interfacial properties using both α and β , thus in the numerical code the dimensional equations 2.1-2.4 are implemented instead.

For the following simulation results, the domain size of the double-periodic computation box is $8\pi \times 8\pi$, and the numerical resolution is 512^2 . The small-scale forcing range is fixed at wavenumbers $5 \leq k/k_0 \leq 15$. At the beginning of each simulation, an initially circular interface of radius 1.5π is placed at the center of a two-dimensional turbulent flow, and the volume average of the concentration is $\langle C \rangle = 0.41 > 0$. The energy spectrum of the turbulent flow is the inverse cascade with a slope of $-5/3$ as shown in figure 1. Throughout the simulations the energy spectrum is little affected by the surface tension force from the interface.

A numerical challenge in turbulent simulations of NS-CH system is that the diffusion coefficient has to be small to avoid phase homogenization. If the diffusion coefficient is too large, or if the surface tension is too small, drops disappear as the order parameter C homogenizes and settles to the phase that is closest to the mean value. Thus, for a given turbulent strength and numerical resolution, we optimize the number of drops by minimizing the diffusion with enough surface tension force so we can collect drops of various sizes. We integrate the turbulent flow over a long duration so the number of drops fluctuates many times around the mean value. The area distributions collected from three simulations with resolution 512^2 , after rescaled with respect to the average drop area, are shown in figure 2(a). The three rescaled area distributions collapse reasonably well in the

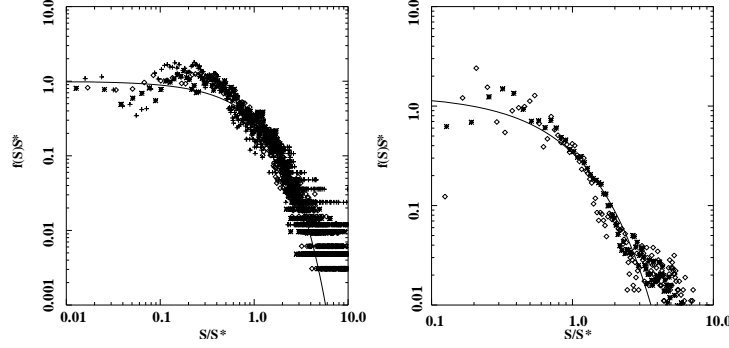


FIGURE 2. Size distribution for simulations of turbulent NS-CH flows. Panel (a): Diamonds are for $\alpha = 2$, $\beta = 200$ and $\mathcal{M} = 10^{-6}$. Crosses are for $\alpha = 2$, $\beta = 200$ and $\mathcal{M} = 5 \times 10^{-7}$. Asterisks are for $\alpha = 3$, $\beta = 300$ and $\mathcal{M} = 10^{-6}$. The numerical resolution is 512^2 and $\nu = 0.1$ for all three simulations, and the curve is $\sim \exp -S/S^*$. Panel (b): Diamonds are for $\alpha = 2$, $\beta = 200$ and $\mathcal{M} = 2 \times 10^{-7}$. Asterisks are for $\alpha = 1.5$, $\beta = 150$ and $\mathcal{M} = 2 \times 10^{-7}$. The numerical resolution is 1024^2 and $\nu = 0.1$ for all both cases, and the curve is $\sim \exp -S/S^*$.

range $0.3 \leq S/S^* \leq 20$, despite the poor statistics at both ends of the distribution. The diffusion coefficients (see caption in figure 2) that we used in the numerical simulations are close to the minimum for this numerical resolution (512^2). 1024^2 grid points are used for two simulations as we decrease the mobility to $\mathcal{M} = 2 \times 10^{-7}$, and similar scaling in the distributions is also found as shown in figure 2(b). Despite the limited reliable range in both figure 2, the general trend suggests that similar scaling may also exist in the turbulent mixing case.

3. Phase-field modeling with zero mobility $\mathcal{M} = 0$

In reality the mobility \mathcal{M} for multiphase flow can be very small, and the equation for the phase field concentration C reduces to the advection transport equation. This distinguished limit corresponds to the non-diffusive, immiscible two-fluid flow, where the interfacial thickness is ideally zero and thus requires special numerical treatment in the simulations.

In the case of zero diffusivity, we use the phase-field modeling as a means to reconstruct the interface knowing its location. We use particle level set method to evolve the interface between the two phases. In the level set framework, the zero of the scalar level set function ϕ implies the location of the interface. To retain the structure of the interface, we assume that the Cahn-Hilliard potential ψ governs the interfacial energetics, and reconstruct the interface for a given interfacial thickness $\xi (= \sqrt{\alpha/\beta})$ as in §2). In §3.1 we formulate this system in terms of level set representation of the interface with phase-field modeling for interfacial structure with zero molecular mobility. In §3.2 we briefly discuss the numerics and some validation is given in §3.3. We then present results from direct numerical simulations of multiphase mixing in two-dimensional turbulence in §3.4.

3.1. Formulation

Basically the equations are exactly the same as those in §2 except the Cahn-Hilliard equation is now reduced to an advection equation for C :

$$\frac{\partial C}{\partial t} + (\mathbf{u} \cdot \nabla)C = 0. \quad (3.1)$$

In the case of vanishing molecular mobility across the interface, the advection transport equation 3.1 for concentration C is a numerical challenge, and more complication arises in the evaluation of the surface tension force. Our remedy is that, despite the non-diffusiveness of the phase field, we assume that the interfacial thickness is finite based on the free energy ψ . Naturally, if we adopt the Cahn-Hilliard surface free energy for ψ , we expect the concentration C to behave as $C \sim \tanh(\sqrt{\beta/\alpha}|r - r_0|)$, where $|\mathbf{r} - \mathbf{r}_0|$ is the distance between the point \mathbf{r} and the interface (located at \mathbf{r}_0). A great advantage of this approach is that the surface tension force can be calculated directly from the phase-field modeling as a continuum force $-C\nabla\psi$, which peaks at the interface.

Thus instead of solving equation 3.1 over the whole computation domain for C , we solve the same equation for a level set function ϕ only at the interface (where $\phi = 0$), and re-initialize the level set function ϕ to a signed distance function away from $\phi = 0$. We replace equation 3.1 with the level set equation valid only at the fluid interface $\phi = 0$:

$$\partial_t \phi + \mathbf{u} \cdot \nabla \phi = 0|_{\phi=0}. \quad (3.2)$$

Away from $\phi = 0$, inside a band of width $\sim 6dx$ around $\phi = 0$, we re-initialize ϕ to a signed distance function. To achieve this we have to re-initialize the level set function at each time step by solving the following equation to a stationary state

$$\partial_\tau \phi + \text{sgn}(\phi_0)(|\nabla \phi| - 1) = 0, \quad (3.3)$$

where $\text{sgn}(\phi_0)$ is the sign of $\phi(\mathbf{x}, t = t_0)$ defined as

$$\text{sgn}(\phi_0) = \frac{\phi_0}{\sqrt{\phi_0^2 + |\nabla \phi_0|^2 dx^2}}, \quad (3.4)$$

for a given grid spacing dx . The normal vector and the mean curvature can be calculated in terms of the level set function ϕ : $\hat{\mathbf{n}} \equiv \nabla \phi / |\nabla \phi|$ and $\kappa \equiv \nabla \cdot \hat{\mathbf{n}}$. The concentration phase-field C is then reconstructed from the level set function (ξ , as previously defined, is the interfacial thickness):

$$C = \tanh\left(\frac{\phi}{\xi}\right) \text{ if } |\phi| \leq a\xi, \quad (3.5)$$

$$C = \frac{\phi}{|\phi|} \text{ if } |\phi| > a\xi,$$

where a is a constant in the range $2 \leq a \leq 5$ so that the concentration C transitions smoothly from $|C| < 1$ to $|C| = 1$ at the edge of the band around the interface. From our fully-resolved simulations of drop dynamics presented here, we conclude that the volume integral of C remains constant at all time provided that the level set is accurately capturing the interface.

Numerically there are various ways to calculate the surface tension force from the level set function. Physically the surface tension force leads to a pressure jump across the interface. In our one-fluid formulation the surface tension is formulated as a body force \mathbf{F}_σ ($= -C\nabla\psi$ in the phase field modeling). Ideally, in the limit of zero interfacial thickness, the surface tension force is non-zero only at the interface: $\mathbf{F}_\sigma = (\sigma\kappa\hat{\mathbf{n}} + \partial_s\sigma\hat{\mathbf{s}})\delta(\phi)$, where $\partial_s\sigma$ is the Marangoni force, with s the arclength and $\hat{\mathbf{s}}$ the unit vectors along the

tangential direction. On a discrete numerical grid, however, the surface tension force F_σ has to be smoothed over several grid spacings to avoid un-controllable numerical oscillation. The usual cosine-delta function used to calculate F_σ on a uniform grid (Sussman *et al.* 1994) leads to artificial broadening of the interface, which in turn leads to large unphysical parasitic currents around the numerically smoothed interface. In our phase field modeling, we assume an interfacial structure based on the the Cahn-Hilliard surface free energy. A continuum surface tension force is then derived based on the surface free energy. As shown in (Jacqmin 1999), this continuum surface tension force gives very small parasitic currents compared with that from the cosine-delta construction of the interface. Recently a numerical scheme has been developed to minimize the parasitic currents (Enright *et al.* 2002). In our approach, the parasitic currents are small but not as minimized as in Enright *et al.* (2002). The turbulent flow in our resolved simulations of drop dynamics is much larger than the parasitic currents, and thus we expect the constraint in Enright *et al.* (2002) to have little effects on the dynamics and drop area distributions presented in §3.4. The formulation we proposed for reconstructing the interface from the phase-field modeling through level set function (equations 3.2-3.5) is somehow similar to the splitting of particle advection from particle diffusion in the random walk particle method (Ghoniem & Sherman 1985). In random walk particle methods, particles can be first transported by the velocity field at their positions, and then perform random walks to account for diffusion. Such a numerical scheme is commonly used in particle tracking when the particle diffusion is very small. Similarly in our formulation we first evolve the interface by solving the advection equation only near the interface using the hybrid particle level set method. Once the location of the interface is advanced and the level set is re-initialized as a signed distance function, we construct the phase-field C based on the steady state solution to equation 2.1 without advecting flow,

$$C(C^2 - 1) - \frac{\alpha}{\beta} \nabla^2 C = 0. \quad (3.6)$$

Assuming that the interfacial structure is only a function of the signed distance to the interface, we then express C in terms of the level set function ϕ in equation 3.5.

In summary, the system of iso-density, iso-viscosity fluid with an interface separating the two phases is described by equations 2.2, 2.3, and 3.2 with the surface tension force $-C\nabla\psi$, where ψ is the Cahn-Hilliard free energy and the concentration C is calculated from equation 3.5.

3.2. Numerics

The level set equation (3.2) is solved using the hybrid particle level set method (Enright *et al.* 2002). We use WENO 5th order scheme to calculate the flux in equation 3.2, and the TVD-3rd order RK scheme to advance the level set in time. Following Enright *et al.* (2002), Lagrangian particles are added inside a narrow band (Γ_p) around the interface and are transported using the same RK 3rd order scheme. Before and after re-initialization (equation 3.3), particle correction (for detail see Enright *et al.* (2002)) is conducted to ensure that the zero level is not shifted numerically. This hybrid level set method is at most volume-conserving as long as particle density along the zero level is sufficient. In all our simulations, we use at least 4^2 particles for each cell within the (Γ_p) band. Re-seeding of particles is conducted if the average particle density is found to be below 75% of the initial particle density. We re-initialize the level set within a second band (Γ_r) enclosing the particle band (Γ_p). We refer readers to Enright *et al.* (2002) for detail of the algorithm. Standard tests have been performed (Young *et al.* 2002) and

results are identical to those in the original paper (Enright *et al.* 2002). To couple the level set equation(s) to the fluid solver, we advance both the level set ϕ and the fluid velocity \mathbf{u} using the 3-rd order explicit scheme. The diffusion part in the momentum equation is incorporated as integrating factors in spectral space. The surface tension force is calculated from the interface at the previous time step, and we use the same velocity fields from the previous time step to advect the velocity, interface, and particles.

3.3. Linear capillary waves

To demonstrate that the surface tension force is properly captured in the phase-field modeling, we compute the oscillatory frequency of the capillary waves for a two-dimensional drop. The initial condition for ϕ is the signed distance function perturbed by a sinusoid with a small amplitude and a wavenumber n

$$\phi(\mathbf{x}, t = 0) = r - r_0(1 + 0.02 \sin(n\theta)), \quad (3.7)$$

where r_0 is the drop radius, $r \equiv |\mathbf{x} - \mathbf{x}_0|$ is the distance between \mathbf{x} and the drop center \mathbf{x}_0 , and $\theta \equiv \tan^{-1}((y - y_0)/(x - x_0))$. Analytically (following Rayleigh (1892)), the oscillation frequency of capillary waves on the interface separating fluids of the same density and zero viscosity ($1/Re = 0$) can be expressed in terms of surface tension coefficient σ , drop radius r_0 , and wavenumber n of the perturbation

$$\omega = \sqrt{\frac{n(n^2 - 1)\sigma}{2r_0^3}}. \quad (3.8)$$

We obtain the linear solutions from simulating the full system (described in section 3.1) with small non-linearity: starting from the initial condition $\mathbf{u} = 0$ and ϕ given in equation 3.7, the non-linearity remains small at all time because the small disturbance is damped by viscosity. In all our simulations in this section, the viscosity ν is fixed at $\nu = 0.1$, and the perturbation amplitude decays exponentially at rate λ with a capillary oscillation of frequency ω . We compute the capillary frequency ω numerically by extracting the oscillation from the decaying amplitude.

We first calibrate the relationship between σ and (α, β) . From §2 the surface tension σ is proportional to $\sqrt{\alpha\beta}$. With the ratio β/α fixed (the interface thickness is thus fixed at ~ 8 grid spacings), we expect the surface tension σ to be linearly proportional to α (or β). Table 3.3 shows the computed oscillation frequency from simulations and the corresponding surface tension coefficient σ from equation 3.8. We find that the surface tension σ (computed from ω in our case via equation 3.8) indeed varies linearly with $\sqrt{\alpha\beta}$.

For $1 \leq n \leq 6$ we compute the oscillation frequency ω from the simulations with $\alpha = 0.9817$ and $\beta = 89.1875$ ($\sigma = 94.32\sigma_0$ from table 3.3). As shown in figure 3, excellent agreement is found between the computed and analytical values of ω for all $1 \leq n \leq 6$. In addition we also remark that the parasitic currents are as small as 10^{-6} with a numerical resolution 128^2 in a square box of size $2\pi \times 2\pi$.

3.4. Drop dynamics in two-dimensional turbulence

Drop dynamics and the drop break-up in simple flow configurations has been extensively investigated both numerically (Zaleski *et al.* 1995; Cristini *et al.* 1998; Tauber *et al.* 2002) and experimentally (Muzzio *et al.* 1991*b*). Results from experiments (Muzzio *et al.* 1991*b*) and modeling (Berthier *et al.* 2001) on passive chaotic mixing of immiscible fluids show that the statistics of drop size collapse due to the self-similar breakup and coalescence

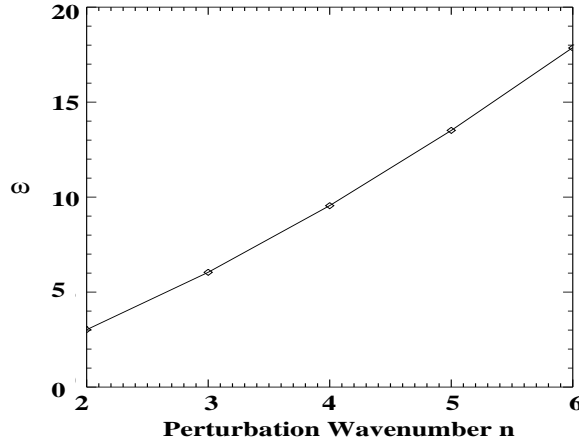


FIGURE 3. Capillary oscillation frequency ω as a function of n . Symbols are simulation data, and line is from analytical result for $\sigma = 94.32\sigma_0$ and $r_0 = \pi$.

TABLE 1. Parameters α and β used in the linear simulations, and the capillary frequency ω computed from the time-varying perturbation amplitude. $n = 2$, $\nu = 0.1$, and numerical resolution is 128^2 .

	α	β	ω	σ/σ_0
Case 1	0.98	89.18	3.02	94.32
Case 2	1.96	178.37	4.24	188.64
Case 3	2.94	267.56	5.22	282.96
Case 4	3.92	356.75	6.04	377.28

processes. However, there are only a few recent direct numerical simulations on drop dynamics in turbulent flows (Tryggvason *et al.* 2001). Due to the difficulty in tracking the interface accurately while conserving fluid mass, it is a great numerical task to capture the statistics of drop size distribution after a series of breakups and coalescence in numerical simulations.

Due to numerical diffusion, it is in general a great numerical challenge to conserve total volume for each fluid using level set methods. The hybrid particle level set method conserves volume almost perfectly in standard tests (Enright *et al.* 2002), and is the only level set method that can both track the interface accurately and minimize the mass loss in a controllable fashion. The particle level set method, in combination with the phase field modeling of the surface tension force, is a good tool for tracking interface accurately with minimum mass loss. Provided that enough Lagrangian particles are used in tracking the interface, the mass loss can be reduced to a tolerable level. Thus we are able to accurately evolve the dynamics of drops in a turbulent flow, and our main goal is to examine the statistics collected from DNS dataset. In our simulations, less than 1% of maximum volume loss is found for all cases presented here. For the following simulation results, the combination of α and β is chosen so that the interface thickness is fixed ($\sim 6dx$ at least). The double-periodic computation domain is of size $8\pi \times 8\pi$, and the numerical resolution is 512^2 .

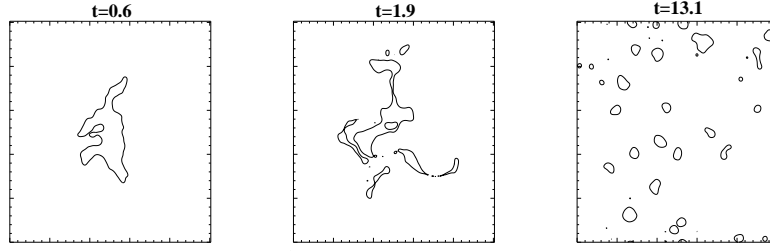


FIGURE 4. Drop deformation and break-up in two-dimensional turbulence. $\alpha = 2.95$, $\beta = 118.92$, $\nu = 0.2$ and $\lambda = 0.1$. (a) $t = 0.6$ (b) $t = 1.9$ and (c) $t = 13.1$.

We fixed the range of small-scale forcing at wavenumbers $5 \leq k/k_0 \leq 15$, and the large scale friction $\mathbf{F}_f = -0.1\mathbf{u}$. At the beginning of each simulation, an initially circular interface of radius π is placed at the center of a two-dimensional turbulent flow. The energy spectrum of the turbulent flow is the inverse cascade with a slope of $-5/3$ as shown in figure 1. Throughout the simulations the energy spectrum is little affected by the surface tension force from the interface. The well-known effect of bubbles/drops on the turbulent energy spectra (Mazzitelli *et al.* 2003) is also absent here because there is no buoyancy/density contrast in our simulations.

In figure 4 we demonstrate how the initial drop gets deformed, stretched, and finally breaks up into smaller drops: In figure 4(a) ($t = 0.6$) the interface is highly distorted, and in figure 4(b) ($t = 1.9$) several break-ups lead to smaller children drops. At late times ($t > 10$) the drops are small and the surface tension force is sufficient to overcome the stretching to prevent further break-ups, and a statistical equilibrium is reached as shown in figure 4(c) ($t = 13.1$), where there are a lot of small drops of irregular shapes and various sizes.

We can easily calculate the total length of the interface from the level set as

$$\begin{aligned} \text{Length}\{\phi = 0\} &= \int_{\Omega} |\nabla H(\phi(\mathbf{x}))| dx dy \\ &= \int_{\Omega} \delta(\phi(\mathbf{x})) |\nabla \phi| dx dy, \end{aligned} \quad (3.9)$$

where

$$H(\phi) = \frac{1}{2} \left[1 + \frac{\phi}{\pi} + \frac{1}{\pi} \sin\left(\frac{\pi\phi}{\epsilon}\right) \right], \quad (3.10)$$

$$\delta(\phi) = \frac{d}{d\phi} H(\phi), \quad (3.11)$$

with $\epsilon = 3 \sim 4dx$ as in Sussman *et al.* (1994). Panel (a) in figure 5 shows the evolution of the arclength (scaled to the initial length), and panel (b) is the time-history of kinetic energy. We find that the early growth in the length is accompanied by a similar growth of the total number of drops as several break-up processes have occurred during ($0 \leq t \leq 3$). After $t \sim 10$ (about 2.5 eddy turnover times) the amplification in length saturates and fluctuates throughout the simulations. We integrate to at least 15 eddy turnover times to attain statistically equilibrium states. The interfacial thickness is fixed at $\sim 6.4dx$ for all three curves in figures 5. With the same small scale random forcing \mathbf{F} , large scale dissipation \mathbf{F}_d and viscous dissipation $\nu = 0.2$, the only difference between the three

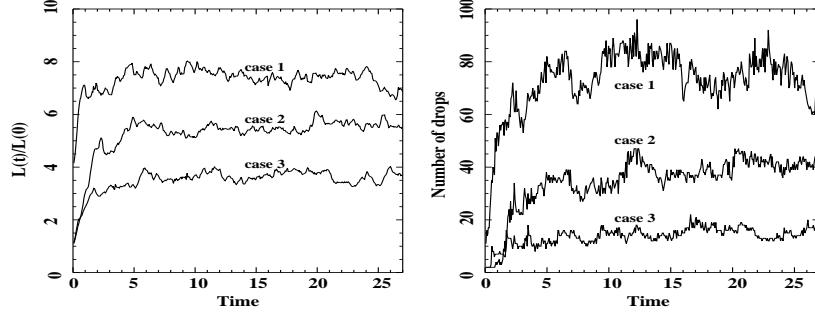


FIGURE 5. (a) Evolution of total arclength scaled to the initial value. (b) Corresponding evolution of number of drops.

TABLE 2. Averaged number of drops and arclengths for the three simulations.

	α	β	σ/σ_0	L/L_0	N
Case 1	1.47	59.45	9.35	7.51	79.98
Case 2	2.94	119.91	18.71	5.50	39.69
Case 3	5.89	239.83	37.42	3.66	15.18

simulations is the surface tension coefficient: $\sigma = 9.36\sigma_0$, $\sigma = 18.71\sigma_0$, and $\sigma = 37.43\sigma_0$ for curves 1, 2, and 3, respectively. (As defined earlier σ_0 is the surface tension coefficient when $\sqrt{\alpha\beta} = 1$.) The balance between stabilizing surface tension force and stirring turbulent flow results in a critical length scale (Lacasta *et al.* 1995)

$$\lambda_c^2 \sim \frac{\pi^2 \sigma}{2 \bar{u}}, \quad (3.12)$$

where \bar{u} is the turbulence characteristic velocity. Since the total area (volume) of each fluid phase has to conserve in two (three)-dimensions, we can estimate the dependence of average number of drops (N) on the surface tension. For a given characteristic turbulence velocity, in two-dimensions,

$$N\lambda_c^2 \sim \text{total area of fluid phase 1} = \text{constant} \rightarrow N \sim \sigma^{-1}. \quad (3.13)$$

Similarly in three-dimensions,

$$N\lambda_c^3 \sim \text{total volume of fluid phase 1} = \text{constant} \rightarrow N \sim \sigma^{-3/2}. \quad (3.14)$$

From equations 3.13 and 3.14, the total circumference (area or arclength in two and three-dimensions, respectively) is inversely proportional to the square root of surface tension: $N\lambda_c$ in two-dimensions and $N\lambda_c^2$ in three-dimensions both lead to $\sim 1/\sqrt{\sigma}$. These scaling results in two-dimensions are consistent with the time-averaged values of our simulation data in figures 5. In table 3.4 we list the time-averaged N and total arclength for all three simulations.

In the statistically equilibrium state the number of drops fluctuates around the mean value, we collect enough statistics for the drop area distribution by integrating over a long period of time. Following Berthier *et al.* (2001) and Muzzio *et al.* (1991b), we rescale the drop area distribution by the mean area (calculate by taking moments of the area

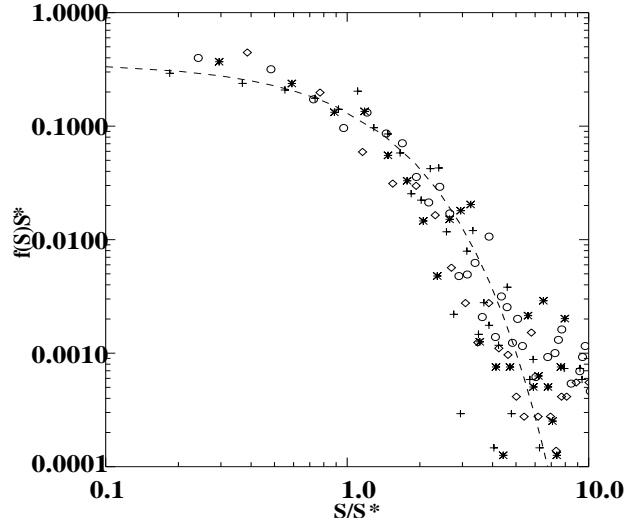


FIGURE 6. Size distribution for the three cases. Diamonds are for case 1, asterisks are for case 2 and crosses are for case 3. Open circles are for a different forcing function but same parameters as in case 1. The dashed line is $\sim \exp -(S/S^*)^2$.

distribution functions as in Muzzio *et al.* (1991b)). Since the effective diffusion coefficient is assumed to be zero in our turbulence simulations, we cannot calculate the mean area based on the scaling of the characteristic domain size L^* and D^* as in Berthier *et al.* (2001). The rescaled area distributions collapse as shown in figure 6. One additional simulation data set (open circles) with a different interfacial thickness and turbulent random forcing is added in figure 6. For this additional simulation, the surface tension $\sigma = 18.71\sigma_0$ and the interfacial thickness $\xi = 5.0dx$ and the turbulent random forcing is at wavenumbers $5 \leq k/k_0 \leq 7.5$, narrower than the other three simulations. However, it seems that the collapse works reasonably well regardless of the differences between the simulations.

4. Conclusion

We have extended the phase-field modeling to the non-diffusive case. Surface free energy from the phase-field modeling is used to calculate the surface tension force based on the reconstructed interface using the level set function. Numerically the non-diffusive, infinitely sharp interface has to be smoothed over a few grid points. Some interfacial structure is always assumed in the numerics, and the resultant surface tension force inherits the modeled structures. One popular way to reconstruct interface in level set method is the cosine-delta function. However, no physical meaning can be related to such a construction, and as a result, the parasitic currents are undesirably large. We replace the cosine-delta function with the smooth interfacial structure from the stationary solution in phase-field modeling, and we calculate the surface tension force from the corresponding surface free energy. The only assumption we make in this approach is that the reconstructed interface is a function of the signed distance to the interface. We assume that “some” molecular dynamics acts on such a fast time scale that the interfacial thickness remains the same, even when the flow is vigorously acting on and around the interface. The collapse of drop area distribution in our two-dimensional turbulence

simulation confirms our conjecture that the self-similar drop area distribution exists for more general velocity fields.

The particle level set method, combined with phase-field modeling, has great promise for large scale, three-dimensional numerical simulations of multiphase flow. One of our future goals is to generalize our simulations of two-dimensional drop dynamics to three dimensions. We also plan to include density and viscosity contrast for multi-fluid using the phase-field modeling. Finally, we are also investigating how the phase-field modeling can be applied in simulating micro-fluidic multiphase flows carried out in experiments (Truesdell *et al.* 2003).

REFERENCES

- BERTHIER, L., BARRAT, J. & KURCHAN, J. 2001 *Phys. Rev. Lett.* **86**, 2014.
 CHELLA, R. & VINALS, J. 1996 *Phys. Rev. E* **53**, 3832.
 CRISTINI, V., BLAWZDZIEWICZ, J. & LOEWENBERG, M. 1998 *Phys. Fluids* **10**, 1781.
 ENRIGHT, D., FEDKIW, R., FERZIGER, J. & MITCHELL, J. 2002 *J. Comp. Phys.* **183**, 83.
 GHONIEM, A. F. & SHERMAN, F. S. 1985 *J. Comput. Phys.* **61**, 1.
 JACQMIN, D. 1999 *J. Fluid Mech.* **155**, 96.
 JAMET, D., TORRES, D. & BRACKBILL, J. 2002 *J. Comp. Phys.* **182**, 262.
 JASNOW, D. & VINALS, J. 1996 *Phys. Fluids* **8**, 660.
 LACASTA, A., SANCHE, J. & SAGUES, F. 1995 *Phys. Rev. Lett.* **75**, 1791.
 MAZZITELLI, I. M., LOHSE, D. & TOSCHI, F. 2003 *Phys. Fluids* **15**, L5.
 MUZZIO, F., SWANSON, P. & OTTINO, J. 1991a *Phys. Fluids* **3**, 822.
 MUZZIO, F., TJAHJADI, M. & OTTINO, J. 1991b *Phys. Rev. Lett.* **67**, 54.
 MUZZIO, F. J., MENEVEAU, C., SWANSON, P. D. & OTTINO, J. M. 1991c *Phys. Fluids* **4**, 1439.
 RAYLEIGH, L. 1892 *Phil. Mag. Science* **34**, 145.
 ROTH, T., FRIEDRICH, C., MARTH, M. & HONERKAMP, J. 2002 *Rheol. Acta* **41**, 211.
 SIGGIA, E. D. 1979 *Phys. Rev. A* **20**, 595.
 SUSSMAN, M., SMEREKA, P. & OSHER, S. 1994 *J. Comp. Phys.* **114**, 146.
 TAUBER, W., UNVERDI, S. O. & TRYGGVASON, G. 2002 *Phys. Fluids* **14**, 2871.
 TRUESDELL, R. A., VOROBIEFF, P. V., SKLAR, L. A. & MAMMOLI, A. A. 2003 *Phys. Rev. E* **67**, 066304.
 TRYGGVASON, G., BUNNER, B., ESMAEELI, A., JURIC, D., AL-RAWAHI, N., TAUBER, W., HAN, J., NAS, S. & JAN, Y. J. 2001 *J. Comp. Phys.* **169**, 708.
 YOUNG, Y.-N., FERZIGER, J., MANSOUR, N., HAM, F. & HERRMANN, M. 2003 *Phys. Fluids* **submitted**.
 YOUNG, Y.-N., HAM, F., MANSOUR, N. & HERRMANN, M. 2002 *CTR Annual Research Briefs* .
 ZALESKI, S., LI, J. & SUCCI, S. 1995 *Phys. Rev. Lett.* **75**, 244.
 ZHAO, P., VENERE, M., HEINRICH, J. C. & POIRIER, D. R. 2003 *J. Comp. Phys.* **188**, 434.